Coupling of Nitric Oxide and Release of Nitrous Oxide from Rare-Earth-Dinitrosyliron Complexes

Arun K. Bar,[†] María José Heras Ojea,[†] Jinkui Tang,[‡,*] Richard A. Layfield[†,*]

[†] Department of Chemistry, School of Life Sciences, University of Sussex, Brighton, BN1 9QJ, U.K.

[‡] Changchun Institute of Applied Chemistry, Chinese Academy of Sciences, Renmin Street 5626, 130022 Changchun, China

Supporting Information Placeholder

ABSTRACT: Addition of Lewis acidic $[Cp^*_2M]^+$ (M = Y, Gd) to the dinitrosyliron complexes (DNICs) $[(NacNac^{Ar})Fe(NO)_2]^-$ (Ar = mesityl, 2,6-diisopropylphenyl) results in formation of the isonitrosyl-bridged DNICs $[(Cp^*)_2M(\mu\text{-}ON)_2Fe(NacNac^{Ar})]$. When Ar = 2,6-diisopropylphenyl, coupling of the NO ligands and release of N_2O occurs. Two factors contribute to this previously unobserved DNIC reactivity mode. Firstly, the oxophilic rare-earth elements drive the formation of isonitrosyl bonds, forcing the DNIC nitrogen atoms into proximity. Secondly, the bulky substituents further squeeze the DNIC, which ultimately overcomes the barrier to NO coupling and demonstrating that N_2O elimination can occur from a single iron centre.

Nitric oxide plays a key role in signalling functions in the cardiovascular system of higher mammals,[1] it is involved in the degradation and re-assembly of iron-sulphur clusters,[2] and it is a reactive nitrogen species involved in nitrosative stress – a process that can lead to cell damage and disease.[3] Removal of intracellular nitric oxide is achieved through the action of flavo-diiron nitric oxide reductase (FNOR), resulting in the formation of nitrous oxide during bacterial denitrification.[4] The mechanism through which two molecules of NO are coupled by FNOR to produce N_2O is the subject of intense discussion.[5,6] The NO coupling step is thought to produce metal-bound hyponitrite, $[N_2O_2]^{2-}$, a process that may involve the ligand forming either in the *cis*- or the *trans*-geometries.[7] Evidence for each pathway has been obtained from studies of enzymes and of biomimetic compounds,[8,9] including structural authentication of bimetallic environments in which the metals are bridged by a hyponitrite ligand.[10]

Dinitrosyliron complexes (DNICs) are important intracellular NO-containing species, small-molecule models of which abound.[11-14] The coupling of the two NO ligands in a monometallic model DNIC to produce N_2O has, however, never been observed. The apparent reluctance of a DNIC to couple two NO ligands is a consequence of the distance between the two nitrogen atoms and the covalent nature of the Fe–NO linkage, which results in a parallel alignment of the unpaired spins, hence the coupling is spin-forbidden.[15,16] Having previously studied the isocarbonyl-bridged rare-earth-iron compounds $[Cp^*_2M\{\mu\text{-}(OC)_2FeCp\}]_2$ (M = Y, Dy),[17] which contain oxophilic $[Cp^*_2M]^+$ units (Cp* = pentamethylcyclopentadienyl), we reasoned that it should be possible to synthesize isonitrosyl-bridged rare-earth-iron compounds in which the DNIC structure is distorted by an oxophilic rare-earth, forcing the NO ligands closer together. The structure-directing influence of the rare-earth could therefore provide a means of overcoming the barrier to NO coupling, leading, potentially, to release of N_2O from the DNIC, thus demonstrating that N_2O release from a monometallic DNIC is indeed possible.

As building blocks for the isonitrosyl bridges, we selected the DNICs $[(NacNac^{Ar})Fe(NO)_2]^-$ in which the iron centre is additionally complexed by the bulky β-diketiminate ligands $[(ArNCMe)_2CH]^-$ (Ar = mesityl, **1a**; 2,6-diisopropylphenyl, **1b**[12]). The reactions of $[Bu_4N]$[**1a**] and $[Bu_4N]$[**1b**] with $[Cp^*_2M][BPh_4]$ (M = Y, Gd) delivered the target isonitrosyl-bridged compounds $\mathbf{2_M}$ and $\mathbf{3_M}$ according to Scheme 1.

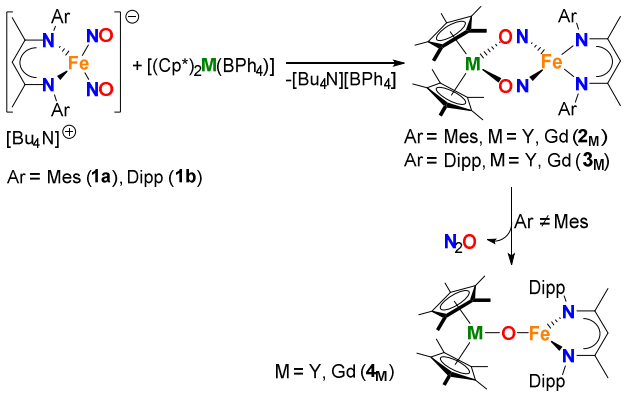

Scheme 1. Synthesis of $\mathbf{2_M}$-$\mathbf{4_M}$ (M = Y, Gd).

Compounds $\mathbf{2_M}$ and $\mathbf{3_M}$ (M = Y, Gd) were isolated in yields of 91%, 93%, 75% and 73%, respectively, and characterized by NMR, IR and UV-visible spectroscopies, in addition to EPR characterization of gadolinium compounds (Figures S1-S21). The molecular structures of the heterobimetallic DNICs were also determined by single-crystal X-ray diffraction (Figures 1, S33, S34, Tables S1-S4), with the core of each consisting of a distorted tetrahedral iron center based on the two nitrogen atoms of the β-diketiminate ligand and the $\{Fe(NO)_2\}^{10}$ DNIC unit (according to Enemark-Feltham notation[18]).

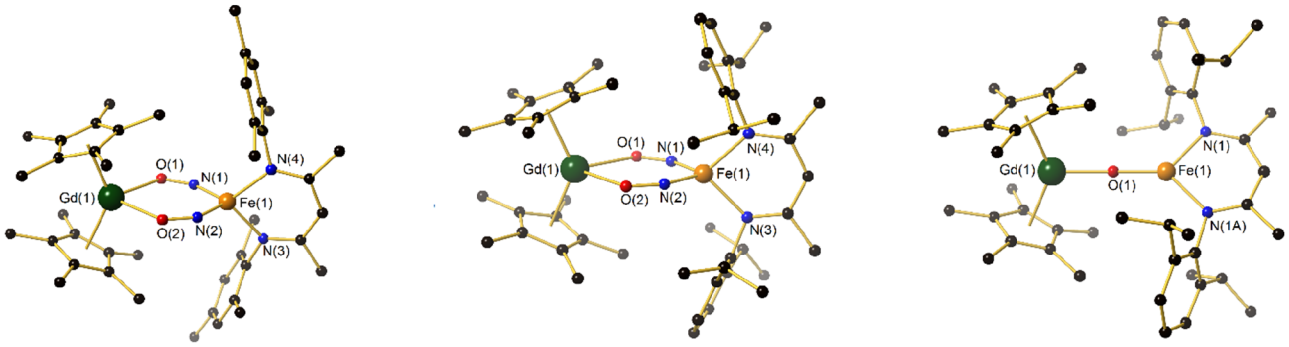

Figure 1. Molecular structures of $\mathbf{2}_{Gd}$ (left), molecule 1 of $\mathbf{3}_{Gd}$ (centre) and $\mathbf{4}_{Gd}$ (right). Hydrogen atoms not shown. Selected bond lengths (Å) and angles (°) for $\mathbf{2}_{Gd}$: Fe(1)–N(1), 1.648(6); Fe(1)–N(2), 1.661(6); N(1)–O(1), 1.239(7); N(2)–O(2), 1.248(7); Gd(1)–O(1), 2.398(5); Gd(1)–O(2), 2.372(5); Y(1)–Cp, 2.352, 2.380; N(1)-Fe(1)-N(2), 95.5(3); Fe(1)-N(1)-O(1), 152.2(5); N(1)-O(1)-Gd(1), 119.3(4); O(1)-Gd(1)-O(2), 82.92(17); Gd(1)-O(2)-N(2), 124.6(4); O(2)-N(2)-Fe(1), 145.4(2); Cp-Gd(1)-Cp, 134.45. For $\mathbf{3}_{Gd}$: Fe(1)–N(1), 1.664(3); Fe(1)–N(2), 1.662(3); N(1)–O(1), 1.253(3); N(2)–O(2), 1.245(3); Gd(1)–O(1), 2.416(2); Gd(1)–O(2), 2.401(2); Gd(1)–Cp, 2.386, 2.381; N(1)-Fe(1)-N(2), 91.34(14); Fe(1)-N(1)-O(1), 148.8(2); N(1)-O(1)-Gd(1), 125.59(19); O(1)-Gd(1)-O(2), 78.57(7); Gd(1)-O(2)-N(2), 124.67(19); O(2)-N(2)-Fe(1), 151.0(3); Cp-Gd(1)-Cp, 134.25. For $\mathbf{4}_{Gd}$: Fe(1)–O(1), 1.774(9); Fe(1)–N(1), 2.007(7); Gd(1)–O(1), 2.044(9), Gd(1)–C, 2.656(7)- 2.734(9); Gd(1)–Cp, 2.415; N(1)-Fe(1)-N(1A), 95.5(4); N(1)-Fe(1)-O(1), 132.25(19); Fe(1)-O(1)-Gd(1), 180.0.

Bending at the nitrosyl nitrogen atoms allows the oxygen atoms to establish isonitrosyl linkages to the rare-earth, which is also bound to two η^5-Cp* ligands.

Beyond the qualitative similarities, important quantitative differences in the key geometric parameters are apparent when comparing $\mathbf{2}_{M}$ and $\mathbf{3}_{M}$. Taking $\mathbf{2}_{Gd}$ and $\mathbf{3}_{Gd}$ as examples, the Fe–N, N–O and Gd–O bond lengths within the {Fe(NO)$_2$Gd} six-membered rings are shorter in $\mathbf{2}_{Gd}$ by 0.003-0.014 Å, 0.003-0.044 Å and 0.003-0.016 Å, respectively, than those in $\mathbf{3}_{Gd}$ (Figure 1). Whereas the sum of the internal angles in the rings are essentially the same for both compounds at approximately 720°, the N-Fe-N and O-Gd-O angles are smaller in $\mathbf{3}_{Gd}$ by 4.2° and 4.3°, respectively. This compression of the isonitrosyl ring in $\mathbf{3}_{Gd}$ increases the Fe···Gd distance by 0.143 Å relative to $\mathbf{2}_{Gd}$ and, significantly, decreases the transannular N···N distance by 0.07 Å. A similar trend is observed for $\mathbf{2}_{Y}$ and $\mathbf{3}_{Y}$, however the differences in the metric parameters are smaller. Structurally authenticated rare-earth-isonitrosyl compounds were, hitherto, unknown, with early reports of such interactions being based on IR spectroscopy.[19,20] The NO stretching frequencies $\tilde{\nu}$(NO) in $\mathbf{2}_{M}$ and $\mathbf{3}_{M}$ occur in the range 1493-1534 cm^{-1} (Figures S11, S13, S17, S19), lower than the analogous values of 1560 and 1623 cm^{-1} determined for the precursor DNICs **1a** and **1b**[12] (Figures S2, S5). These spectral features are consistent with the greater Fe-N-O bending angles of 144.43(2)-152.2(5)° and the longer N–O distances of 1.239(7)-1.253(3) Å in $\mathbf{2}_{Gd}$ and $\mathbf{3}_{Gd}$, which compare to the analogous angles of 163.4(2)° and 170.8(3)°, and distances of 1.216(3) and 1.210(3) Å, in **1a**. The compressed nature of the dinitrosyliron unit in $\mathbf{3}_{Gd}$ is further highlighted when compared with the structure of the precursor **1b**,[12] which has the same Fe–N bond lengths but an N-Fe-N angle of 109.2(2)° and an N···N separation of 2.703 Å, which are wider and longer by substantial margins of 17.9° and 0.324 Å, respectively. These observations further highlight the remarkable flexibility of the {Fe(NO)$_2$}^{10} DNIC unit, with the primary geometric distortions accompanying the formation of $\mathbf{2}_{M}$ and $\mathbf{3}_{M}$ being directed by the oxophilic rare-earth element. The differing steric demands of the β-diketiminate mesityl and diisopropylphenyl substituents can therefore be regarded as producing secondary structural distortions, which has implications for the stability of $\mathbf{3}_{M}$ with respect to the elimination of N$_2$O (see below).

Whilst $\mathbf{2}_{Y}$ and $\mathbf{3}_{Y}$ are diamagnetic, $\mathbf{2}_{Gd}$ and $\mathbf{3}_{Gd}$ are paramagnetic with $\chi_M T$ values of 7.86 and 7.71 cm^3 K mol^{-1}, respectively, at 300 K (χ_M is the molar magnetic susceptibility), the slight variation in this quantity with temperature being characteristic of Gd^{3+} (Figures S36, S38).[21] The field dependence of the magnetization, $M(H)$, for $\mathbf{2}_{Gd}$ and $\mathbf{3}_{Gd}$ is also characteristic of Gd^{3+}, reaching values of 7.11 and 6.73 μ_B at 1.9 K and 7 T (Figures S37, S39). Based on ^{1}H NMR spectroscopy, toluene solutions of diamagnetic $\mathbf{2}_{Y}$ are stable indefinitely at room temperature and show no sign of decomposition when heated to 100°C in toluene (Figure S22). In contrast, green solutions of $\mathbf{3}_{M}$ in toluene turn brown-yellow after stirring for five days at room temperature. The sharp resonances observed in the ^{1}H NMR spectrum of diamagnetic $\mathbf{3}_{Y}$ (Figure S16) broaden and become distributed over chemical shifts ranging from +119.5 ppm to –151.2 ppm, indicating paramagnetism (Figures S23, S24). GC-MS analysis of the headspace gas after stirring confirmed that N$_2$O is produced during this process (Figure S25). For $\mathbf{3}_{M}$, filtration of the solutions obtained after stirring, subsequent concentration and cooling to 0°C resulted in the formation of yellow crystals of the oxo-bridged compounds [Cp*$_2$M(μ-O)Fe(NacNac^{Dipp})] ($\mathbf{4}_{M}$) (M = Y, Gd), which were isolated in yields of 72% and 78%, respectively (Scheme 1).

Analysis by X-ray diffraction revealed that complexes $\mathbf{4}_{M}$ are isostructural and consist of a three-coordinate iron center in a distorted trigonal-planar environment (Figures 1, S35). The μ-oxo link to the rare-earth metal coincides with a crystallographic two-fold rotation axis and, hence, the Fe-O-M angle is 180.0° in both complexes. The {Cp*$_2$M} units in $\mathbf{4}_{M}$ adopt bent metallocene structures similar to those in $\mathbf{2}_{M}$ and $\mathbf{3}_{M}$. The magnetic susceptibility of $\mathbf{4}_{Y}$ shows a $\chi_M T$ value of 5.63 cm^3 K mol^{-1} at 300 K and a magnetization of 2.89 μ_B at 1.9 K and 7 T, which suggest a high-spin S = 2 iron(II) with an appreciable orbital contribution to the magnetic moment (Figures S40, S41). A satisfactory fit of the susceptibility data could not be achieved using a standard spin Hamiltonian, which may indicate that the large orbital contribution originates from mixing of a low-lying electronic excited state into the ground state, a phenomenon that has previously been observed in closely related three-coordinate iron(II) complexes.[22,23] An approximate fit of the $\chi_M T(T)$ data yielded a large, negative axial zero-field splitting parameter of $D \approx -28(1)$ cm^{-}

^{1} and $g \approx 2.6(1)$ (Figure S40), similar to the values determined for other three-coordinate iron(II) compounds.[24] The $\chi_M T$ value for $\mathbf{4_{Gd}}$ at 300 K is 12.54 cm^3 K mol^{-1}, which gradually decreases down to 20 K before increasing to 14.84 cm^3 K mol^{-1} at 2 K, indicating ferromagnetic coupling between Gd^{3+} and Fe^{2+} (Figures S42, S43). A fit of the data was achieved using an exchange coupling constant of J = +0.25 cm^{-1} (–2J formalism), along with g_{Gd} = 2.00, g_{Fe} = 2.49 and D_{Fe} = –18.3 cm^{-1}.[25]

The chemistry of model DNICs and related systems is well-established, with many examples providing insight into the mechanisms through which NO is transported and delivered *in vivo*.[26,27] The removal of NO from biological systems as N_2O involves a coupling reaction in the active site of FNOR,[28] which consists of a non-heme, carboxylate-bridged diiron environment that has been studied as diiron-dinitrosyl and diiron-mononitrosyl model compounds, some of which produce N_2O under conditions of chemical or electrochemical reduction.[29-31] In contrast, N_2O elimination from a DNIC has not previously been observed. The reluctance of DNICs to couple the two NO ligands is thought to be due very strong antiferromagnetic exchange coupling between iron and NO, which results in a parallel alignment of spins on the nitrogen atoms and, hence, a substantial barrier to N–N bond formation.[15] In the case of $\mathbf{3_M}$, the steric bulk imposed on the isonitrosyl $\{M(ON)_2Fe\}$ cores by the diisopropylphenyl substituents helps to overcome this barrier by forcing the nitrogen atoms much closer together than in mesityl-substituted 2_M, and the ensuing nitrosyl coupling and elimination of nitrous oxide proceeds under mild conditions. The systems described here are clearly different to naturally occurring iron-nitrosyl complexes, yet when the biological N_2O elimination reaction in its most elementary form, i.e. $2NO + 2e^- + 2H^+ \rightarrow N_2O + H_2O$,[6] is compared to the synthetic analogue $\{Fe(NO)_2\}^{10} + [Cp^*_2M]^+ \rightarrow N_2O + \{Cp^*_2MOFe\}^+$, similarities are apparent since the DNIC unit can provide the required number of electrons to couple the NO ligands. The instability of $\mathbf{3_M}$ with respect to the formation of $\mathbf{4_M}$ and N_2O is significant since the reactivity shows that conversion of NO to N_2O can occur at a single iron center, the first time that such reactivity has been demonstrated. Furthermore, the formation and subsequent reactivity of $\mathbf{3_M}$ showcases the structural flexibility of the DNIC unit in the presence of a strongly Lewis acidic rare-earth organometallic fragment, which forces the nitrogen atoms into the correct conformation to allow NO coupling and N_2O release. These observations provide a potential blueprint for the design and synthesis of other heterobimetallic DNICs capable of releasing N_2O.

ASSOCIATED CONTENT

Supporting Information

The Supporting Information is available free of charge on the ACS Publications website. Synthesis, spectroscopic characterization, crystallography details, magnetic property measurements.

AUTHOR INFORMATION

Corresponding Authors

r.layfield@sussex.ac.uk
tang@ciac.ac.cn

Notes

The authors declare no competing financial interests.

ACKNOWLEDGEMENT

The authors thank the Royal Society for a Newton International Fellowship to AKB (NF160853) and a Newton Advanced Fellowship to JT (NA160075). For financial support, RAL thanks the European Research Council (CoG RadMag, grant 646740) and the EPSRC (EP/M022064/1), and JT thanks the National Natural Science Foundation of China (grants 21525103 and 21871247). The authors are grateful to Mr. D. Fehn and Prof. K. Meyer (Friedrich-Alexander University Erlangen-Nürnberg) for measuring the EPR spectra of compounds $\mathbf{3_{Gd}}$ and $\mathbf{4_{Gd}}$.

REFERENCES

(1) Fitzpatrick, J.; Kim, E. Synthetic Modeling Chemistry of Iron-Sulfur Clusters in Nitric Oxide Signaling. *Acc. Chem. Res*. **2015**, *48*, 2453–2461.

(2) Crack, J. C.; Green, J.; Thomson, A. J.; Brun, N. E. L. Iron-Sulfur Clusters as Biological Sensors: The Chemistry of Reactions with Molecular Oxygen and Nitric Oxide. *Acc. Chem. Res*. **2014**, *47*, 3196–3205.

(3) Farah, C.; Michel, L. Y. M.; Balligand, J.-L. Nitric Oxide Signalling in Cardiovascular Health and Disease. *Nat. Rev. Cardiol*. **2018**, *15*, 292.

(4) Lu, J.; Bi, B.; Lai, W.; Chen, H. Origin of Nitric Oxide Reduction Activity in Flavo–Diiron NO Reductase: Key Roles of the Second Coordination Sphere. *Angew. Chem. Int. Ed*. **2019**, *58*, 3795–3799.

(5) Kindermann, N.; Schober, A.; Demeshko, S.; Lehnert, N.; Meyer, F. Reductive Transformations of a Pyrazolate-Based Bioinspired Diiron–Dinitrosyl Complex. *Inorg. Chem*. **2016**, *55*, 11538–11550.

(6) Lehnert, N.; Fujisawa, K.; Camarena, S.; Dong, H. T.; White, C. J. Activation of Non-Heme Iron-Nitrosyl Complexes: Turning Up the Heat. *ACS Catal*. **2019**, *9*, 10499–10518.

(7) Van Stappen, C.; Lehnert, N. Mechanism of N–N Bond Formation by Transition Metal–Nitrosyl Complexes: Modeling Flavodiiron Nitric Oxide Reductases. *Inorg. Chem*. **2018**, *57*, 4252–4269.

(8) Kundu, S.; Phu, P. N.; Ghosh, P.; Kozimor, S. A.; Bertke, J. A.; Stieber, S. C. E.; Warren, T. H. Nitrosyl Linkage Isomers: NO Coupling to N_2O at a Mononuclear Site. *J. Am. Chem. Soc*. **2019**, *141*, 1415–1419.

(9) Hayashi, T.; Caranto, J. D.; Wampler, D. A.; Kurtz, D. M.; Moënne-Loccoz, P. Insights into the Nitric Oxide Reductase Mechanism of Flavodiiron Proteins from a Flavin-Free Enzyme. *Biochemistry*. **2010**, *49*, 7040–7049.

(10) Ferretti, E.; Dechert, S.; Demeshko, S.; Holthausen, M. C.; Meyer, F. Reductive Nitric Oxide Coupling at a Dinickel Core: Isolation of a Key Cis-Hyponitrite Intermediate En Route to N_2O Formation. *Angew. Chem. Int. Ed*. **2019**, *58*, 1705–1709.

(11) Pulukkody, R.; Kyran, S. J.; Bethel, R. D.; Hsieh, C. H.; Hall, M. B.; Darensbourg, D. J.; Darensbourg, M. Y. Carbon Monoxide Induced Reductive Elimination of Disulfide in an *N*-Heterocyclic Carbene (NHC)/Thiolate Dinitrosyl Iron Complex (DNIC). *J. Am. Chem. Soc*. **2013**, *135*, 8423–8430.

(12) Tonzetich, Z. J.; Do, L. H.; Lippard, S. J. Dinitrosyl Iron Complexes Relevant to Rieske Cluster Nitrosylation. *J. Am. Chem. Soc*. **2009**, *131*, 7964–7965.

(13) Tonzetich, Z. J.; McQuade, L. E.; Lippard, S. J. Detecting and Understanding the Roles of Nitric Oxide in Biology. *Inorg. Chem*. **2010**, *49*, 6338–6348.

(14) Tinberg, C. E.; Tonzetich, Z. J.; Wang, H.; Do, L. H.; Yoda, Y.; Cramer, S. P.; Lippard, S. J. Characterization of Iron Dinitrosyl Species Formed in the Reaction of Nitric Oxide with a Biological Rieske Center. *J. Am. Chem. Soc*. **2010**, *132*, 18168–18176.

(15) Speelman, A. L.; Zhang, B.; Silakov, A.; Skodje, K. M.; Alp, E. E.; Zhao, J.; Hu, M. Y.; Kim, E.; Krebs, C.; Lehnert, N. Unusual Synthetic Pathway for an $\{Fe(NO)_2\}^9$ Dinitrosyl Iron Complex (DNIC) and Insight into DNIC Electronic Structure via Nuclear Resonance Vibrational Spectroscopy. *Inorg. Chem*. **2016**, *55*, 5485–5501.

(16) Ye, S.; Neese, F. The Unusual Electronic Structure of Dinitrosyl Iron Complexes. *J. Am. Chem. Soc*. **2010**, *132*, 3646–3647.

(17) Pugh, T.; Chilton, N. F.; Layfield, R. A. A Low-Symmetry Dysprosium Metallocene Single-Molecule Magnet with a High Anisotropy Barrier. *Angew. Chem. Int. Ed*. **2016**, *55*, 11082-11085.
(18) Enemark, J. H. Principles of Structure, Bonding and Reactivity for Metal Nitrosyl Complexes. *Coord. Chem. Rev*. **1974**, *13*, 339–406.
(19) Crease, B. A. E.; Legzdins, P. The Lewis Acidity of Organolanthanides. The Interaction of Cyclopentadienyl-Lanthanides with Some Carbonyl and Nitrosyl Complexes. *J. Chem. Soc., Dalton Trans*. **1973**, 1501-1507.
(20) Crease, A. E.; Legzdins, P. The Lewis Acidity of Organolanthanides. Evidence for Isocarbonyl and Isonitrosyl Complex Formation. *J. Chem. Soc. Chem. Commun*. **1972**, 268–269.
(21) Tuna, F.; Smith, C. A.; Bodensteiner, M.; Ungur, L.; Chibotaru, L. F.; McInnes, E. J. L.; Winpenny, R. E. P.; Collison, D.; Layfield, R. A. A High Anisotropy Barrier in a Sulfur-Bridged Organodysprosium Single-Molecule Magnet. *Angew. Chem. Int. Ed*. **2012**, *51*, 6976–6980.
(22) Lin, P. H.; Smythe, N. C.; Gorelsky, S. I.; Maguire, S.; Henson, N. J.; Korobkov, I.; Scott, B. L.; Gordon, J. C.; Baker, R. T.; Murugesu, M. Importance of Out-of-State Spin-Orbit Coupling for Slow Magnetic Relaxation in Mononuclear Fe^{II} Complexes. *J. Am. Chem. Soc*. **2011**, *133*, 15806–15809.
(23) Andres, H.; Bominaar, E. L.; Smith, J. M.; Eckert, N. A.; Holland, P. L.; Münck, E. Planar Three-Coordinate High-Spin Fe^{II} Complexes with Large Orbital Angular Momentum: Mössbauer, Electron Paramagnetic Resonance, and Electronic Structure Studies. *J. Am. Chem. Soc.* **2002**, *124*, 3012–3025.
(24) Layfield, R. A.; McDouall, J. J. W.; Scheer, M.; Schwarzmaier, C.; Tuna, F. Structure and Bonding in Three-Coordinate N-Heterocyclic Carbene Adducts of Iron(II) *Bis*(Trimethylsilyl)Amide. *Chem. Commun*. **2011**, *47*, 10623-10625.
(25) Chilton, N. F.; Anderson, R. P.; Turner, L. D.; Soncini, A.; Murray, K. S. PHI: A Powerful New Program for the Analysis of Anisotropic Monomeric and Exchange-Coupled Polynuclear d- and f-Block Complexes. *J. Comput. Chem*. **2013**, *34*, 1164–1175.
(26) Hess, J. L.; Hsieh, C. H.; Reibenspies, J. H.; Darensbourg, M. Y. N-Heterocyclic Carbene Ligands as Mimics of Imidazoles/Histidine for the Stabilization of Di-and Trinitrosyl Iron Complexes. *Inorg. Chem*. **2011**, *50*, 8541–8552.
(27) Speelman, A. L.; Lehnert, N. Heme versus Non-Heme Iron-Nitroxyl $\{FeN(H)O\}^8$ Complexes: Electronic Structure and Biologically Relevant Reactivity. *Acc. Chem. Res*. **2014**, *47*, 1106–1116.
(28) Caranto, J. D.; Weitz, A.; Hendrich, M. P.; Kurtz, D. M. The Nitric Oxide Reductase Mechanism of a Flavo-Diiron Protein: Identification of Active-Site Intermediates and Products. *J. Am. Chem. Soc*. **2014**, *136*, 7981–7992.
(29) Feig, A. L.; Bautista, M. T.; Lippard, S. J. A Carboxylate-Bridged Non-Heme Diiron Dinitrosyl Complex. *Inorg. Chem*. **1996**, *35*, 6892–6898.
(30) Zheng, S.; Berto, T. C.; Dahl, E. W.; Hoffman, M. B.; Speelman, A. L.; Lehnert, N. The Functional Model Complex $[Fe_2(BPMP)(OPr)(NO)_2](BPh_4)_2$ Provides Insight into the Mechanism of Flavodiiron NO Reductases. *J. Am. Chem. Soc*. **2013**, *135*, 4902–4905.
(31) Jana, M.; Pal, N.; White, C. J.; Kupper, C.; Meyer, F.; Lehnert, N.; Majumdar, A. Functional Mononitrosyl Diiron(II) Complex Mediates the Reduction of NO to N_2O with Relevance for Flavodiiron NO Reductases. *J. Am. Chem. Soc*. **2017**, *139*, 14380–14383.

TOCs graphic